Available online at www.sciencedirect.com

SciVerse ScienceDirect

Physics Procedia 41 (2013) 20 – 30

Physics Procedia

Lasers in Manufacturing Conference 2013

Spatter formation in laser welding with beam oscillation

M. Schweier*, J. F. Heins, M. W. Haubold, M. F. Zaeh

Institute for Machine Tools and Industrial Management, Technische Universitaet Muenchen, Boltzmannstraße 15, 85748 Garching, Germany

Abstract

The investigation presented in this paper aims on a quantitative analysis of spatter formation in laser beam welding with superposed beam oscillation. After a discussion of design space limitations, which result from the scanner dynamics and theoretical considerations on the welding process itself, an optimal experimental design is created. By the use of high speed camera imaging, spatters were captured during statistically designed welding experiments and correlations between the number of spatters and the welding parameters have been derived. To evaluate the spatter characteristics in the high speed videos, a state space approach was applied, which is based on automated image data processing.

Keywords: laser beam welding; machine vision; spatter formation; design of experiments; beam oscillation; high speed camera; Kalman filter; multihypothesis tracking

1. State of the Art and Motivation

Laser beam welding of metallic materials is becoming more and more flexible, since fiber lasers with multi-kilowatt output power and almost single mode beam divergence ($M^2 < 1.3$) are available. The high quality radiation of these beam sources can nearly be focused to its diffraction limit, which results in peak intensities of over 1 MW/mm^2 on the workpiece's surface. [1; 2] With those high intensities very deep and narrow weld seams can be produced at common welding speeds of a few m/min [1; 3; 4]. Unlike in welding with moderately focused multi mode laser radiation, the process of melting and vaporization and thus the formation of a keyhole is kept up even at considerably higher welding speeds [4]. Consequently, high power single mode laser radiation is preferably used in welding with superposed beam oscillation, wherein the laser spot is moved with high and alternating speed on the oscillation trajectory. The preservation of a vapor capillary at high speed is particularly important when single mode fiber lasers are used, because with these the dimensions of the oscillation trajectory can be larger when compared to the focal diameter of the laser beam and thus the melt

* Corresponding author. Tel.: +49 89 289 15470
E-mail address: markus.schweier@iwb.tum.de

doi:10.1016/j.phpro.2013.03.047

pool. Several recent publications of experimental results attest, that laser welding with superposed beam oscillation offers major advantages over conventional laser welding in certain applications.

BEREND ET AL. [5] introduced a newly developed 1D scanning system for oscillation frequencies of up to 1.5 kHz. By using this system in welding the aluminum alloy EN AW-5182, it was shown that the number and size of pores in the weld seam, which particularly occur at higher welding speeds, could be significantly reduced at high oscillation frequencies. Furthermore, they observed that beam oscillation can help to reduce the surface roughness of the seam, which is in good accordance with the findings of [6] and [7], who presented a miniaturized, highly dynamic scanning system for laser beam micro welding. In welding experiments on optical fiber arrays, consisting of the zinc-containing alloy CuNi18Zn20, the process stability could be increased by the use of high-frequency beam oscillation, resulting in fewer melt ejections and a stable deep welding process. The surface roughness of the weld seams on the fiber arrays could be reduced from an average of Ra = 5 µm to an average of Ra = 2.5 µm [6]. REITER ET AL. [8] conducted a study on spiking, which is a common failure in electron and laser beam welding with strongly focused radiation, and quantitatively verified that spiking is obviously lower when beam oscillation is used. In [9] and [10] another laser welding optics for high-frequency beam oscillation was presented, which can be used in combination with high power single mode fiber laser radiation. The authors used this optics to join the dissimilar material combination of aluminum and copper in lap and butt joint configuration. Through optimized process parameters they were able to produce weld seams, which almost reached the weld seam strength of the weaker base material aluminum, though the formation of intermetallic phases could not be prevented. In a further publication an exemplary comparison of spatter formation in welding with and without superposed beam oscillation on different materials was drawn and it was proven that by far fewer spatters occurred at an oscillation frequency of 4 kHz when welding mild steel as well as an aluminum alloy [11].

Whereas spatter formation in conventional laser welding (without beam oscillation) has been experimentally investigated by several researchers [12–15] for both CO_2 and solid state laser radiation, no conclusive study exists on this topic for welding with superposed beam oscillation. Hence, this paper aims at a quantitative analysis of spatter formation in laser welding with superposed beam oscillation. Therefore, the idea of JÄGER ET AL. [16] is adopted. They developed an algorithm for a process monitoring system, based on coaxial imaging of the processing zone, to detect spatters in conventional laser welding. In order to extract quantitative information on the spatter characteristics during the laser welding process, the data extracted by the algorithm is further correlated with processing parameters by means of a design of experiments (DOE) study. Hereby a descriptive process model, which helps to understand spatter formation in laser welding with superposed beam oscillation, is derived. This model in turn can help to establish sound process windows.

2. Experimental and Computational Approach

When scanners are used to superpose the welding speed v (oriented along the x-direction) with an oscillating beam motion, the laser beam is moved on a trajectory, which is generally defined by equation (1).

$$\vec{p} = \begin{pmatrix} x \\ y \end{pmatrix} = \begin{pmatrix} v \cdot t + A_x \cdot \sin\left(2 \cdot \pi \cdot f_x \cdot t + \varphi_x\right) \\ A_y \cdot \sin\left(2 \cdot \pi \cdot f_y \cdot t + \varphi_y\right) \end{pmatrix} \quad (1)$$

Therein x and y are the time-dependent laser spot coordinates, A_i are the oscillation amplitudes, f_i are the oscillation frequencies and φ_i the respective phase angles in x- and y-direction [17]. The oscillation form is determined by the frequency ratio f_x / f_y and the phase shift $\Delta\varphi = \varphi_x - \varphi_y$. To ensure a harmonic, recurring movement the frequency ratio needs to be rational. Within this paper all presented investigations are restricted to the circular oscillation form, which results for equal amplitudes ($A_x = A_y$), equal frequencies ($f_x / f_y = 1$) and a

phase shift of $\pi / 2$, since this is the most frequently used form in industrial practice. An example of the trajectory for a circular oscillation is given in Fig. 1 (left).

Fig. 1 (right) shows the black box representation of the experimental investigation. The welding parameters laser power P and welding speed v as well as the oscillation parameters amplitude A and frequency f are varied. Since not every possible combination of the processing factors in the set design space either makes sense from a welding perspective or can be realized by the experimental set-up, two restrictions are derived. Those restrictions and the resulting test plan are explained in detail in section 2.2. The experimental set-up used for the welding study is documented in section 2.1. To characterize the spatter behavior of the welding process, a quantitative measurand is needed. Due to practical considerations the specific average number of spatters per unit length n is chosen. Its automated determination from high-speed camera images is described in section 2.2. All weldments were produced on the stainless steel grade X5CrNi18-10 (1.4301).

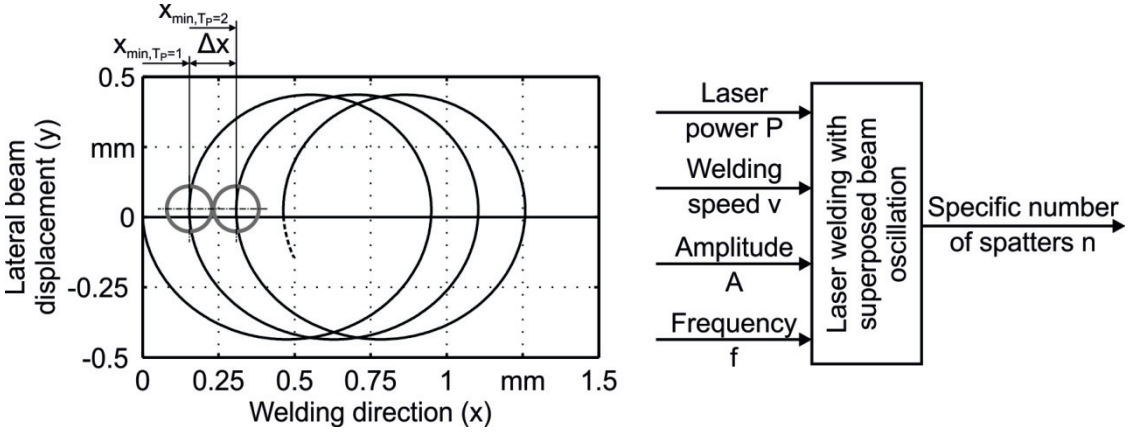

Fig. 1. Beam displacement during the first three periods of a circular laser beam oscillation with $v = 150\ mm/s$, $f_x = f_y = f = 971\ Hz$, $A_x = A_y = A = 0.44\ mm$ and $\Delta\varphi = \varphi_x - \varphi_y = \pi/2$ (left) and black box representation of the experimental investigation (right)

2.1. Experimental set-up

All experiments were conducted using the set-up shown in Fig. 2. The radiation was generated by an ytterbium-doped YAG single mode (SM) fiber laser by IPG Photonics. This laser source emits continuous wave (cw) radiation with a maximum output power of $P_{max} = 3\ kW$ at a wavelength of $\lambda = 1070\ nm$. As per the data sheet of the manufacturer, the emitted radiation is almost diffraction-limited ($M^2 < 1.25$) at all power levels. The radiation was guided to the scanner optics (1) through an optical fiber with a core diameter of $d_c = 30\ \mu m$. The oscillating beam displacement was created by a modified Remote Welding Elephant from ARGES with an aperture of 36 mm and a focal length of approx. 550 mm. This post-objective scanner optics has further been equipped with weight optimized mirrors, which had been fabricated of SiC. The optical magnification of the scanning system is 1.66, thus the nominal focus diameter in the working plane is $d_f = 50\ \mu m$. Since high-speed camera imaging requires a stationary process zone (8), the feeding motion was realized by a rotating movement. The welding specimens were clamped onto a turntable (7), which was driven by an electric motor (6). Using this arrangement, the processing zone always stays in the view field of the high-speed camera (2). The type iSpeed 3 high-speed camera by Olympus features a monochrome CMOS sensor with a maximum resolution of 1280 x 1024 pixels. The image sequences presented within this paper were recorded at a frame rate of 7500 fps and a resolution of 636 x 476, which was found to be an appropriate trade-off between temporal and spatial resolution for spatter recognition. To ensure a good contrast between the

background of the image and the spatters, an 810 nm wavelength filter (3) was used. The high-speed camera was fixed perpendicular to the material surface, so that the distortion of the images was negligible.

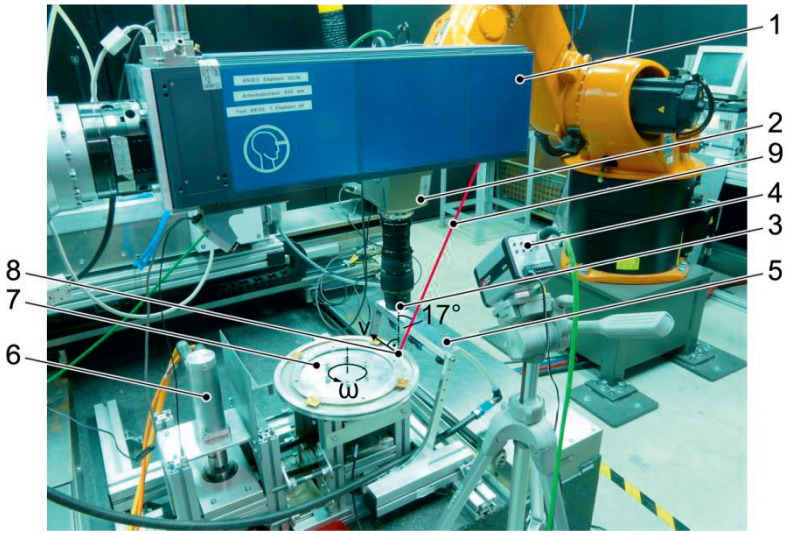

Pos.	Component
1	Scanner optics
2	High-speed camera
3	Wavelength filter (810 nm)
4	Process monitoring camera
5	Cross jet
6	Electric drive
7	Turntable
8	Process zone
9	Laser beam

Fig. 2. Experimental set-up for spatter analysis by high-speed camera imaging

2.2. Design of experiments (DOE)

There are two major reasons why DOE was used for the investigation. The first one is that high-speed camera imaging produces vast amounts of data. Every recorded sequence, which is used for the analysis of one factor combination, contains approx. 6750 images with 250 kB each, which corresponds to a time period of 0.9 s. To reduce the amount of data, that needs to be recorded, transferred to a computer, stored and processed, the number of experimental runs needs to be minimized. At the same time the informative value of the study needs to be guaranteed. The second reason is that a quantitative correlation of processing parameters and the number of spatters shall be established. DOE meets both previously stated requirements and was therefore chosen for this analysis. The investigated parameter ranges are given in Table 1.

Processing Parameter	Minimum	Maximum	Unit
Laser power P	1000	3000	W
Welding speed v	16.67	150	mm/s
Oscillation frequency f	200	1910	Hz
Oscillation amplitude A	0.2	0.75	mm

Table 1. Parameter ranges of the experimental design

Within the design space given above certain sectors were additionally excluded, resulting in restrictions, with which the test plan had to comply. On the one hand a restriction was set for the minimum required frequency f_{min} as a function of the welding velocity v. As theoretically discussed by [17], the frequency f needs to increase with the welding velocity v in order to ensure an appropriate energy deposition over the complete weld seam area. This requirement applies in particular to the case of the presented experimental set-up, since the focus diameter d_f of the single mode laser beam is small when compared to the dimensions of the oscillation

trajectory (A). During laser welding with beam oscillation the track speed of the laser spot changes permanently and can reach values of several thousand mm/s, depending on the welding velocity v and the oscillation parameters [2]. From previous welding experiments without beam oscillation for welding speeds v up to 4000 mm/s it is known that the smallest width of the molten area in the weld seam, which was measured in cross section polishes, is approx. 0.1 mm. Based on this the restriction (2) is formulated, which says, that the distance Δx in welding direction travelled during one oscillation period T_P needs to be smaller than the minimum expected melt pool width (0.1 mm). For better understanding the distance Δx is plotted in Fig. 1. Since the oscillation period T_P is the reciprocal of the frequency f, a relationship between v and f is thus established, which can be used as the first design space restriction. This restriction is shown in Fig. 3 (left).

$$\Delta x = x_{\min,T_P=2} - x_{\min,T_P=1} \overset{!}{\geq} v \cdot T_P = \frac{v}{f} \tag{2}$$

A second restriction results from the limited dynamics of the scanning system. Based on the method presented in [2], the scanner optics used in this study was analyzed in order to derive a descriptive model of the maximum possible oscillation frequency, which can be run until shortly before the scanner is shut-off to prevent overheating of the galvanometer drives. It was found that this maximum frequency solely depends on the set amplitude A, as given in Fig. 3 (center).

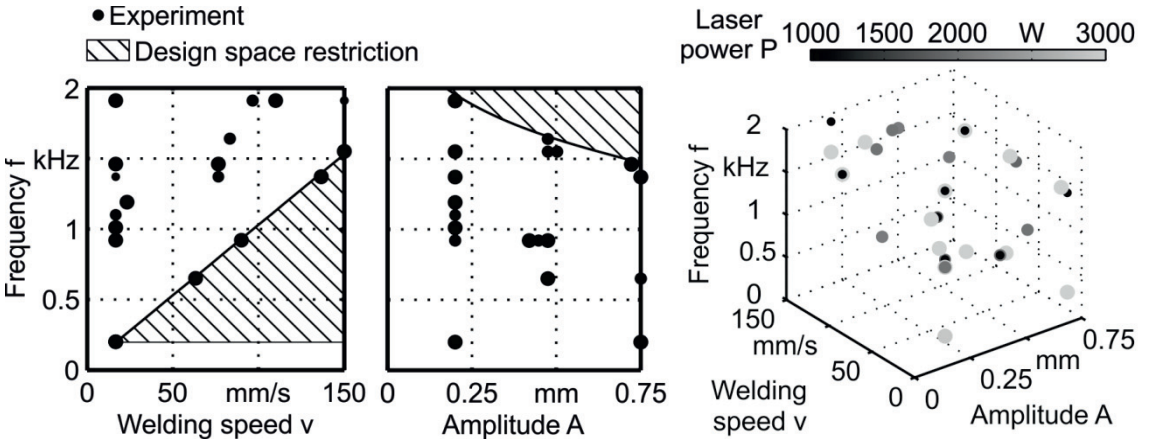

Fig. 3. Design space restrictions, resulting from the welding process (left) and limited scanner dynamics (center) and a four-dimensional representation of the restricted experimental design with 50 experiments (right) (laser power represented by bubble color and size)

With the factor ranges given in Table 1 and the design space restriction shown in Fig. 3 (left + center) it was possible to develop a suitable test plan. Since the whole design space had to be covered, the first 25 experimental points were set quasi-equally distributed, using an algorithm based on the Latin Hypercube Sampling. Furthermore, these 25 experimental points were augmented with 25 A-optimal[†] points, which were computed according to [18], to ensure good statistical properties[‡] of the test plan despite the design space

[†] In an A-optimal design the experimental points are set, so that the trace of the matrix $(X'X)^{-1}$ is minimized, wherein X is the design matrix. This ensures a minimum mean variance of the regression coefficients and is therefore a good choice, in case the effects and the significance of the different parameters are totally unknown.

[‡] All variance inflation factors (VIFs) of the experimental design are smaller than 6.5, assuming a 2nd degree polynomial regression equation.

restrictions. The final test plan with the 50 experimental points used for the welding study is graphically illustrated in Fig. 3 (right).

2.3. Image data processing

The following section briefly describes the functionality of the program used for spatter tracking in the high-speed image sequences of the laser welding experiments. It is based on the idea of [16] and was adapted from the open source code of WAUTHIER available online at [19]. Its main processing steps are given in Fig. 4.

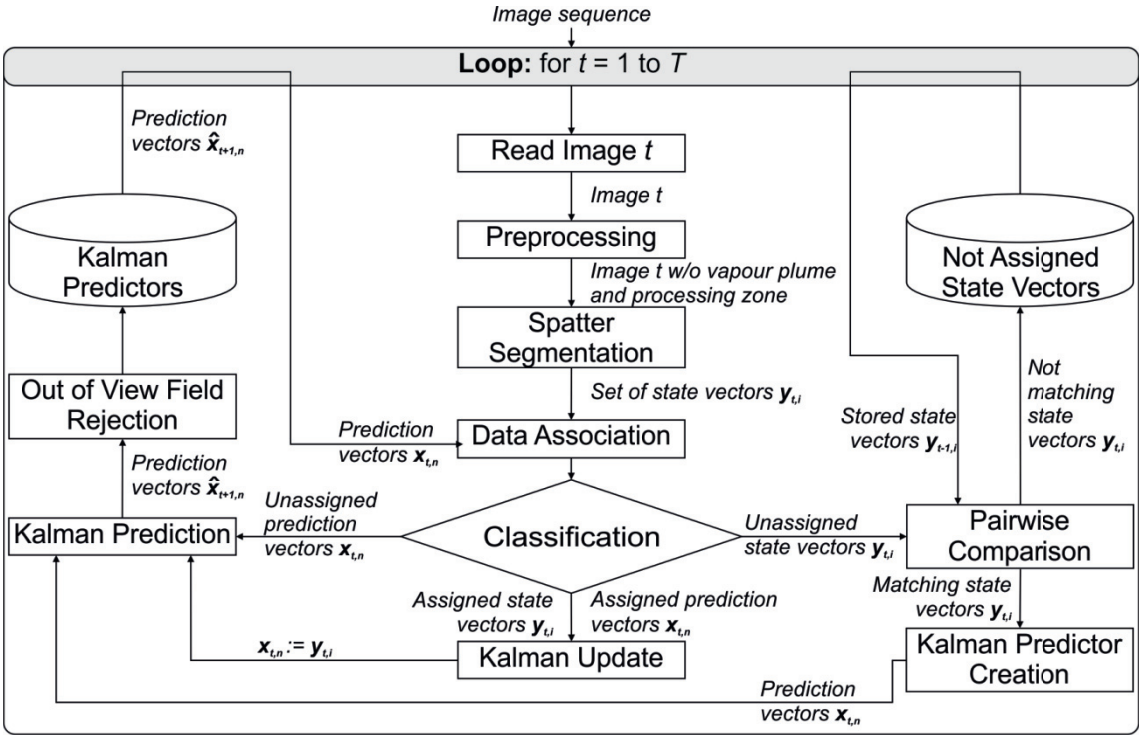

Fig. 4. Flow chart of the program for spatter analysis, with image number t, total image number T, prediction vectors $\boldsymbol{x}$ and state vectors $\boldsymbol{y}$

The core element of the algorithm is the use of a Kalman filter in combination with a multihypothesis assignment solver, which is also known as multihypothesis tracking (MHT) in this context. The program runs in a loop over t until all available images T in the sequence have been processed. First of all the image t is read and preprocessed to eliminate the vapor plume, which flows out of the capillary and the processing zone. This is done by subtracting a diffused copy of the image from the original. After this step the spatters are segmented by a sequence of edge detection and thresholding operations. The result is a set of regions, which represent possible spatters in the current image. These regions are further quantified with their state vectors $\boldsymbol{y_{t,i}}$. These state vectors as well as the Kalman prediction vectors are of the form given in (3), wherein p_x and p_y are the coordinates of the i^{th} object's center of gravity, v_x and v_y are the corresponding velocities and s is the region size.

$$y_{t,i} = \begin{pmatrix} p_x & p_y & v_x & v_y & s \end{pmatrix}^T \tag{3}$$

The next step is to assign the segmented objects to already existing predictions, which have been computed during the processing of the previous image. These predictions are calculated with the linear state space model $\boldsymbol{A}$, which assumes a motion with constant velocity and is given in (4).

$$\hat{x}_{t+1,i} = A \cdot x_{t,i} \text{ with } A = \begin{pmatrix} 1 & 0 & 1 & 0 & 0 \\ 0 & 1 & 0 & 1 & 0 \\ 0 & 0 & 1 & 0 & 0 \\ 0 & 0 & 0 & 1 & 0 \\ 0 & 0 & 0 & 0 & 1 \end{pmatrix} \quad (4)$$

To assign the recognized regions and their state vectors $\boldsymbol{y_{t,i}}$ to the Kalman prediction vectors $\boldsymbol{x_{t,i}}$ a linear assignment problem is formulated. The solver minimizes a cost function consisting of the summation of the assignment costs of three states[§]. For further information on the algorithm for solving these kinds of linear assignment problems please refer to [20].

There are three possible results after the assignment step. The first is that an appropriate pair of state and prediction vector can be found. In this case the values in the prediction vector are updated with the measured values from the state vector and a new Kalman prediction for the subsequent image is calculated using equation (4). The second possible outcome of the assignment step is that a prediction vector could not be assigned. This typically happens in object tracking, if the tracked object is hidden behind something or the images are overlain by strong random noise. In this case a new prediction for the subsequent image is calculated from the current prediction. In the program presented here, the allowed number of predictions without a successful assignment is set to 10 frames. Thereafter the trajectory is automatically ended. The third and last case is that a state vector could not be assigned to any Kalman prediction vector. This particularly occurs, when new spatters are ejected from the processing zone. In this case the program tries to match this state vector to another state vector, which could not be assigned during the previous image. If this attempt is successful, a new prediction vector is calculated from the two assigned state vectors. Otherwise it is stored for this kind of comparison in the subsequent image. At last all unassigned, updated and newly formulated prediction vectors are used to calculate predictions for the subsequent image and are checked against the size of the view field. The same procedure is repeated with the next image.

Fig. 5 shows an example for a randomly selected image series after the spatter recognition. In image 290 a new region is segmented for the first time, after a spatter was ejected from the processing zone. In the subsequent frame 291 the spatter is detected for a second time and a Kalman prediction (52) vector is thus created. In the following frame a new prediction for this spatter is created and used for recognition. It is worth to mention that the algorithm even works well, when several spatters are moving in a similar direction with different velocities (e.g. spatters 48 – 50).

[§] As segmentation in one frame does not provide any information on the velocity of the spatter, the corresponding components in the state vector are always zero.

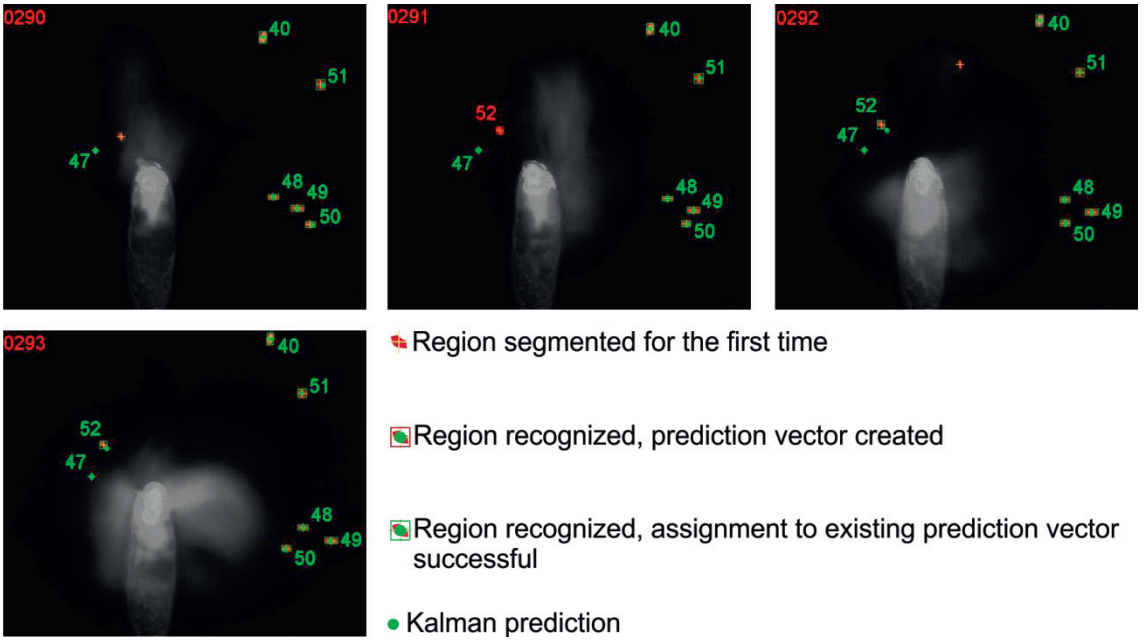

Fig. 5. Recognized spatters in an exemplary image series

3. Results and Discussion

Using the spatter trajectories computed form the image data of the welding experiments, the specific average number of spatters per unit length n was derived as a practical measurand of the spatter behavior. It was found that this measurand varied significantly from a minimum of 0 mm^{-1} to a maximum of almost 32 mm^{-1} within the investigated design space. Since the system behavior was totally unknown and scattering of the measured values needed to be expected a stepwise analysis of variances (ANOVA) [18] was used to derive an empirical model and to remove insignificant factors methodically. As negative predictions of the response variable (n) could be excluded based on practical considerations, the response variable was transformed using the method of BOX & COX [21] so that

$$n_i^* = \frac{\left(n_i^{\lambda} - 1\right)}{\lambda} \text{ with } \lambda = \frac{1}{2} \tag{5}$$

As it is difficult to illustrate the correlations of all four factors, the results of the ANOVA are given in the form of an interaction plot in Fig. 6. In this plot every diagram displays how two factors interact. In particular every diagram contains the predicted values of the specific number of spatters against one factor, while another factor is set at one high and one low level and the others are kept constant at their medium level.

The regression model revealed several basic relationships. The first one is that the laser power and the welding velocity have the strongest influences on the number of spatters, almost independent of how the oscillation parameters are chosen (s. plots VII – XII). The higher the laser power, the higher is the specific number of spatters. This is particularly important as a higher laser power is needed to increase the welding width or depth, which in turn is often a requirement in industrial practice. A second general statement from this analysis is that the specific number of spatters strongly decreases with increasing welding velocity (s. diag. II,

V, XII). This coincides with the common requirement of low processing times and is in particular distinctive at higher laser powers. But again this relationship can be interpreted as a downside, since high welding velocities usually come with lower welding depths and furthermore require for higher scanner dynamics, since the required minimum oscillation frequency increases at higher welding velocities [2; 7].

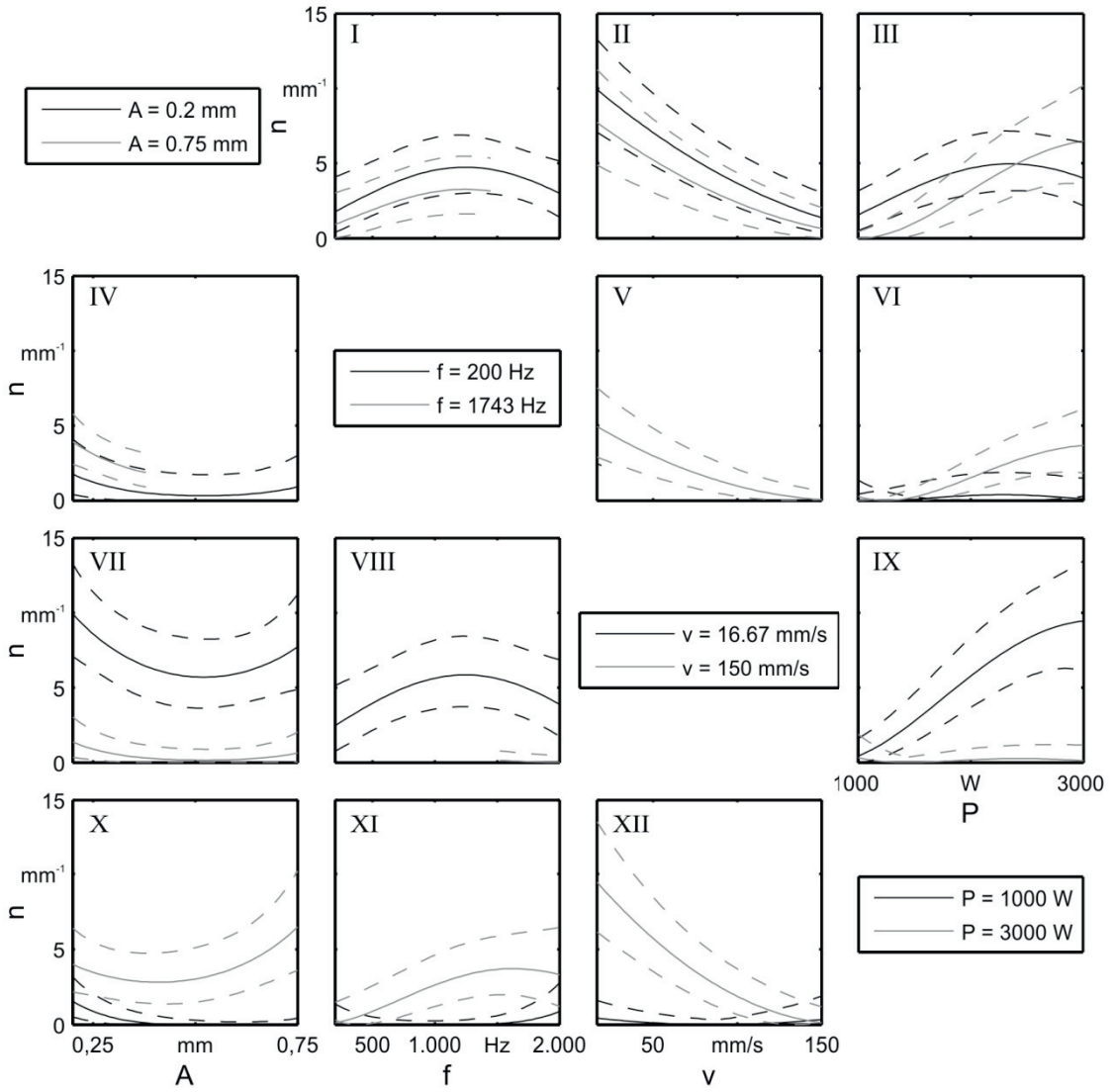

Fig. 6. Interaction plot of the regression model for spatter prediction with oscillation amplitude *A*, oscillation frequency *f*, welding velocity *v* and laser power *P* (predicted values: solid lines, 90 % confidence intervals: dashed lines; restricted parts of the design space are not plotted)

Moreover, the regression model predicts interesting interactions between the oscillation amplitude and the other factors. In any case the predicted number of spatters is higher for the small amplitude level, except at laser powers above approx. 2.500 W (s. diag. I, II, III). This observation can be explained as follows: Using

smaller oscillation amplitudes, the laser power is distributed to a smaller material volume, which leads to a more concentrated energy input. Thereby the molten material may be overheated and thus the formation of spatters is increased. In contrast, coming from a local minimum the number of spatters seems to increase again at higher amplitudes (s. diag. IV, VII, X), which can be explained by the high speed videos. At certain welding parameters the laser spot exits and re-enters the subsequent melt pool once during every oscillation period. As the laser spot re-enters the melt pool, it imposes a sudden momentum on the melt, which leads to a small melt explosion once during every period. This suggests that the amplitude needs to be chosen with care, so that it is high enough to prevent excessive heat input on the one hand. On the other hand the amplitude needs to be small enough, so that the laser spot does never exit the melt pool during the oscillation. The influence of the frequency was found to be rather low when compared to the other factors. No interaction of the frequency and the welding velocity resulted from the regression analysis. But as the design space was restricted with a linear correlation of frequency and welding velocity, no clear statement on the interaction of those two factors can be made.

4. Conclusions

With today's fiber lasers and scanner optics laser beam welding has become more and more flexible. Amongst others the laser beam oscillation technique, which is already applied in certain industrial applications, is one of the new possibilities that scanner optics offer. This technique has been applied in several experimental studies, but no investigation on its influence on the spatter behavior in laser beam welding had been presented. In this paper an approach to model the relationship between welding and oscillation parameters as well as the specific average number of spatters per unit length was presented. To measure the spatter behavior, high speed camera images were recorded during statistically planned welding experiments. An object tracking algorithm, based on a Kalman filter and a multihypothesis assignment solver, was used to extract the spatter trajectories from the image series. The results of the processed image data was used as input for a regression analysis in order to derive an empirical model for the prediction of the number of spatters as a function of laser power, welding velocity, oscillation amplitude and frequency. The regression revealed that the laser power and the welding velocity have the strongest influence on the number of spatters. In particular it was found that the number of spatters decreases with increasing welding velocity and increases with increasing laser power, whereas the influence of the oscillation frequency is minor.

Acknowledgements

A part of the results presented in this paper was developed within the research project RoboLaSS, which is funded by the German Federal Ministry of Education and Research (BMBF). The authors express their due gratitude for the funding.

References

[1] Beyer E, Mahrle A, Lütke M, Standfuss J, Brückner F. Innovation in high power fiber laser applications. In: Beyer E, editor. *SPIE Photonics West 2012 - Proceedings of LASE*, San Francisco; 2012, pp. 1–11

[2] Schweier M, Zaeh MF, Reppich J, Hatwig J. Single Mode Fiber Laser Beam Welding with Superposed Beam Oscillation. In: Laser Institute of America, editor. *Proceedings of the 30th International Congress on Applications of Lasers & Electro-Optics*, Orlando: LIA Pub; 2011, pp. 536–546

[3] Seefeld T, Vollertsen F. Welding with Single Mode Fibre Lasers. In: Fraunhofer IWS, editor. *International Lasersymposium Fiber and Disc (FiSC 2006)*, Stuttgart: Fraunhofer Verlag; 2006

[4] Musiol J, Lütke M, Schweier M, Hatwig J, Wetzig A, Zaeh, M, Beyer E: Combining Remote Ablation Cutting and Remote Welding - Opportunities and Application Areas. In: Beyer E, editor. *SPIE Photonics West 2012 - Proceedings of LASE*, San Francisco; 2012, pp. 82390Q1-Q14

[5] Berend O, Haferkamp H, Meier O, Engelbrecht L. High-frequency Beam Oscillating to Increase the Process Stability during Laser Welding with High Melt Pool Dynamics. In: Laser Institute of America, editor. *Proceedings of the 24th International Congress on Applications of Lasers & Electro-Optics*, Orlando: LIA Pub; 2005, pp. 1032–1041

[6] Schmitt F, Funck M, Boglea A, Poprawe R. Development and application of miniaturized scanners for laser beam micro-welding. *Microsyst Technol* 2008; **14**:1861–1869.

[7] Poprawe R, Schmitt F, Mehlmann B, Olowinsky A, Gillner A. Systemtechnik zur örtlichen Leistungsmodulation beim Laserstrahl-Mikroschweißen. In: Vollertsen F, Büttgenbach S, Kraft O, Michaeli W, editors. *4. Kolloquium Mikroproduktion*, Bremen: BIAS-Verlag; 2009

[8] Reiter MJ, Cho J, Farson DF, Mehl M. Analysis and Control of Penetration Depth Fluctuations in Single-Mode Fiber Laser Welds. In: Laser Institute of America, editor. *Proceedings of the 28th International Congress on Applications of Lasers & Electro-Optics*, Orlando: LIA Pub; 2009, pp. 800–809

[9] Kraetzsch M, Standfuss J, Klotzbach A, Berndt B, Beyer E. Laser Beam Welding with High-Frequency Beam Oscillation - Welding of dissimilar materials with Brilliant Fiber Lasers. In: Laser Institute of America, editor. *Proceedings of the 30th International Congress on Applications of Lasers & Electro-Optics*, Orlando: LIA Pub; 2011, pp. 169-178

[10] Kraetzsch M, Standfuss J, Klotzbach A, Kaspar J, Brenner B, Beyer E. Laser Beam Welding with High-Frequency Beam Oscillation - Welding of Dissimilar Materials with Brilliant Fibre Lasers. In: Schmidt M, Zaeh MF, Graf T, Ostendorf A, editors. LiM - Lasers in Manufacturing 2011 Part 1, Munich: Elsevier Science; 2011, pp. 142–149

[11] Standfuß J, Beyer E. Innovations in laser welding using high brightness lasers. In: Fraunhofer IWS, editor. *International Lasersymposium Fiber and Disc (FiSC 2012)*, Stuttgart: Fraunhofer Verlag; 2012

[12] Weberpals J, Dausinger F. Influence of Inclination Angle on Spatter Behavior at Welding with Lasers of Strong Focusability. In: Laser Institute of America, editor. *Proceedings of the 26th International Congress on Applications of Lasers & Electro-Optics,* Orlando: LIA Pub; 2007, pp. 858-865

[13] Kaplan AF, Powell J. Laser Welding: The Spatter Map. In: Laser Institute of America, editor. *Proceedings of the 29th International Congress on Applications of Lasers & Electro-Optics,* Orlando: LIA Pub; 2010, pp. 683-690

[14] Cai H, Xiao R. Comparison of Spatter Characteristics in Fiber and CO_2 Laser Beam Welding of Aluminium Alloy. In: Laser Institute of America, editor. *Proceedings of the 30th International Congress on Applications of Lasers & Electro-Optics*, Orlando: LIA Pub; 2011, pp. 150–158.

[15] Gärtner P, Weber R. Spatter Formation and Keyhole Observation with High Speed Cameras - Better Understanding of the Keyhole Formation. In: Laser Institute of America, editor. *Proceedings of the 28th International Congress on Applications of Lasers & Electro-Optics*, Orlando: LIA Pub; 2009, pp. 339-342.

[16] Jäger M, Humbert S, Hamprecht FA. Sputter Tracking for the Automatic Monitoring of Industrial Laser-Welding Processes. *IEEE Transactions on Industrial Electronics* 2008; **55**:2177–2184.

[17] Mahrle A, Beyer E. Modelling and Simulation of the Energy Deposition in Laser Beam Welding with Oscillatory Beam Deflection. In: Laser Institute of America, editor. *Proceedings of the 26th International Congress on Applications of Lasers & Electro-Optics,* Orlando: LIA Pub; 207, pp. 714–723

[18] Siebertz K, Hochkirchen T, van Bebber D. *Statistische Versuchsplanung*. 1st ed. Berlin, Heidelberg: Springer; 2010.

[19] Wauthier F. Motion Tracking in Image Sequences. online available: *http://www.cs.berkeley.edu/~flw/tracker/* (11/26/2012)

[20] Jonker R, Volgenant A. A shortest augmenting path algorithm for dense and sparse linear assignment problems. *Computing* 1987;**38**:325–340.

[21] Box GEP, Cox, DR. An Analysis of Transformation. *Journal of the Royal Statistical Society* 1964; **26**:211–252.